Moliner Marin, M.; Gabay, JE.; Kliewer, CE.; Serna Merino, PM.; Corma Canós, A. (2018). Trapping of Metal Atoms and Metal Clusters by Chabazite under Severe Redox Stress. ACS Catalysis. 8(10):9520-9528. https://doi.org/10.1021/acscatal.8b01717

Trapping of Metal Atoms and Metal Clusters by Chabazite under Severe REDOX Stress

Manuel Moliner,[a]* Jadeene Gabay,[b] Chris Kliewer,[b] Pedro Serna,[b]* Avelino Corma[a]*

[a] Instituto de Tecnología Química, Universitat Politècnica de València-Consejo Superior de Investigaciones Científicas, Avenida de los Naranjos s/n, 46022 València, Spain

[b] ExxonMobil Research and Engineering Co., Annandale, New Jersey 08801, United States

*corresponding authors: mmoliner@itq.upv.es, pedro.m.serna-merino@exxonmobil.com, acorma@itq.upv.es

Many industrial processes rely on supported transition metal catalysts to carry out chemical transformations. Highly dispersed metal nanoparticles on supports are often preferred, not only because of their excellent properties for the activation of H_2,(*1*) O_2,(*2*) H_2O and CO_2,(*3*), and a plethora of organic moieties,(*4*) but also because they are relatively stable against metal sintering under most reaction conditions. Nonetheless, many processes operate at particularly harsh conditions (pressure, temperature and/or redox stress) to overcome kinetic or thermodynamic limitations, conditions under which most industrial catalysts suffer metal deactivation and, more specifically, metal sintering. Then, to reestablish the properties of the fresh materials, complex rejuvenation protocols must often be developed (e.g. oxychlorination).(*5*) Therefore, the design of noble metal catalysts that are not only active and selective, but highly stable in a variety of atmospheres, is a major industrial challenge that demands more practical solutions.

Sintering is particularly problematic when the metal is noble in character (i.e. Pt, Pd) and the reactive atmosphere includes oxidizing components.(*6-8*) Coalescence (Brownian motion), which occurs mostly in reducing atmospheres, can be relatively easily controlled by using supports with pores and cavities, such as zeolites,(*9-11*) or encapsulation techniques.(*12*) Unfortunately, O_2 enables Ostwald-ripening sintering mechanisms that these types of materials are usually unable to suppress. Stability under oxidizing conditions is important in a number of high temperature chemistries (e.g. oxidation of CO for exhaust catalysis), but also in processes where metal catalysts must be periodically re-activated by calcination to remove coke deposits.(*13*)

Paradoxically, the first steps of sintering by Ostwald-Ripening, that is, the release of single metal atoms from small to large particles (to cause a loss of dispersion), is the basis for metal re-dispersion in other cases.(*14*) Ripening occurs when big (thermodynamically more stable) particles in the catalyst trap the metal atoms released by the small particles after their fragmentation. But if the support provides Strong Metal Support Interactions (SMSI),(*15*) such as those typically observed on reducible supports such as CeO_2 or TiO_2, the mobile metal species can be intercepted before further aggregation phenomena occur, limiting or eliminating the problem. Based on this principle, for example, CeO_2 added to Pt/Al_2O_3 catalysts results in a remarkable improvement of the sinter-resistant performance in the combustion of CO after harsh O_2 aging steps.(*16*)

Herein, we demonstrate that Al-containing CHA zeolite is as a very efficient non-reducible metal-trap that prevents Ostwald-ripening under severe conditions in O_2, even when the noble metal precursors are deposited on a second surface (e.g. SiO_2 or Al_2O_3). In this scenario, the massive irreversible metal-sintering typically observed with non-reducible supports (including zeolites) due to volatile MO_x species is largely circumvented. The methods, surface-chemistry and overall sinter-resistant characteristics appear to be applicable to a family of metal-containing CHA samples, for example, Pt, Pd, and bimetallic Pt-Pd combinations. This opens the door to unconventional metal structures inside zeolites (i.e. single atoms and small metal clusters) under conditions where they usually do not exist in favor of bulk-like particles. These metal-based CHA catalysts show excellent performance when compared to industrially practiced Pt-Al_2O_3 in applications where severe redox stress exist, such as the water gas-shift (WGS) reaction.

In a recent paper, we have demonstrated that Pt inside a Si-rich small crystal CHA, made via a direct synthesis method (i.e. the zeolite is crystalized in the presence of a metal complex), shows outstanding sinter-resistant characteristics in both H_2 and O_2, as well as high hydrothermal stability in the presence of steam.(*10*) More Al-rich small pore zeolites, such as LTA, in contrast, displayed lower hydrothermal stability.(*10*) The metal structure was shown to convert stoichiometrically, and in a reversible manner, from clusters (0.8-1.5 nm in diameter) to single Pt atoms, as the gas composition was cycled between H_2 and O_2 (Figure S1).(*10*) The stability of the single metal atoms in O_2 at temperatures as high as 650°C is remarkable, especially if one considers that a) CHA is a non-reducible support where SMSI interactions (such as those commonly observed with TiO_2 or CeO_2) cannot be invoked, and b) the coulombic interactions between cations and Al sites in zeolites are, in general, insufficient to avoid Ostwald-Ripening of noble metals under the conditions investigated in the present paper (see Figure S2 with Pt/ZSM-5 as an illustrative example). Relevant examples of single-atom Pt and Pd catalysis on TiO_2 or CeO_2, or Cu clusters in a variety of zeolites have been recently reported.(*17-19*)

The energetic barrier for single Pt atoms to cross through the 8-ring window of CHA appears to be relatively low, as the temperature needed to turn single atoms into 20-to-100-atoms clusters in H_2 is <200°C.(*10*) We infer, thus, that the remarkable stability of single Pt atoms in O_2 is not (at least not exclusively) related to the constrained cage-like structure of this zeolite. Although the exact nature of the binding sites in CHA that allow suppression of Ostwald-Ripening sintering remains

unresolved, our EXAFS data show that the single Pt atoms resulting from a high temperature O_2 treatment (e.g. 550°C) are bonded to 3-4 oxygen atoms in the first coordination sphere (Entry 2 of Table S1). If CHA can indeed trap PtO_x, one should then be able to develop synthesis protocols based on wetness methods (instead of a one-pot approach (*10*)), coupled with a high temperature O_2 activation, to achieve very high Pt dispersions inside the CHA crystals, and even single metal atoms. In this sense, wetness techniques, such as ion-exchange, are by far the most common laboratory and industrial methods for the synthesis of metal-containing zeolites, but it is broadly accepted that the incorporation of noble metals into the channels and cavities of small-pore zeolites using these methods is impractical, because solvated metal precursors are too large to diffuse into the material before big metallic particles precipitate.(*20*) This problem is more acute for metals like Pt, Pd, Rh and Ir (*20*) than for Cu and Ni.(*21, 22*) However, we observe that some Al-CHA samples exposed to aqueous $Pt(NH_3)_4(NO_2)_2$, dried, and subsequently calcined in O_2 at 650°C (see SI for experimental details) do not reveal signs of agglomeration by SEM (Figure S3), with optimal results obtained when the Al-CHA crystals are small and the Al density is relatively high (see comparative examples in Figure S3, Pt/CHA-8 vs Pt/CHA-12_exc and Pt/CHA-25_exc). EXAFS confirms the absence of Pt-Pt interactions in the ion-exchanged small crystal Pt/CHA-8 after the high temperature calcination (see Pt/CHA in Figure 1, and Table 1). In fact, the EXAFS data suggest the presence of species spectroscopically indistinguishable from those contained at this stage in the Pt/CHA sample made via the one-pot method (on average, a Pt-O c.n. of 3-4 at 2.01 Å is inferred, see Table 1). Subsequent reduction of the metal in H_2 at 400°C leads, moreover, to small metal nanoparticles with diameters in the range 0.8-1.5 nm, as in the one-pot sample (see STEM image of Pt/CHA-8 in Figure 2a). Actually, the overall oxidation-reduction performance of the ion-exchanged sample and the previously reported one-pot material is virtually identical (see STEM image in Figure S1a), with full reversibility between clusters and single atoms through the severe redox cycles. The performance in shape-selective ethylene/propylene hydrogenations further demonstrates that the metal in the ion-exchanged sample is also located in the interior of the CHA crystals (Figure S4).

We then postulated that the choice of $Pt(NH_3)_4(NO_2)_2$, a complex that exceeds the dimensions of the CHA 8-ring windows (the $Pt(NH_3)_4$ unit is ~5 Å, whereas the CHA apertures are ~ 0.38 nm), to synthesize the sinter-resistant material should be of relative minor importance, if one accepts that PtO_x species likely form in O_2 at these high temperatures independently of the metal source. One option, based on our observation that small metal particles fully fragment into PtO_x species at

temperatures in the range 550-650°C (*10*), would be to start from Pt nanoparticles located on the outer surface of the small crystal CHA before any thermal treatment (see Scheme 1 in Figure S5 and SI for experimental details). As hypothesized, subsequent treatment of this sample with O_2 at 650°C caused the metal particles to re-disperse (see STEM images in Figure S6b). Small clusters (~ 1 nm) reappeared later when the sample was exposed to H_2 at 400°C (Figure S6c), very much as if we had started the redox process from the one-pot Pt/CHA (see STEM image in Figure S1a) or the $Pt(NH_3)_4(NO_2)_2$ ion-exchanged samples (see STEM image in Figure 2a).

The mobility of PtO_x on supports has been discussed previously in the literature.(*6, 23-25*) They can spillover the support and move as weakly bonded surface species, but they can also become volatile, provided that the temperature is high enough. At temperatures >400°C (we note that this threshold is a rough approximation, as several factors, such as the nature of the support, the metal, and the size of the metal ensembles, may affect the volatility of the metal species), these volatile Pt species have been proposed to travel among support particles, which aggravates the sintering problem.(*6, 25*) In agreement, we detect agglomeration in 0.3 wt % Pt/SiO_2 when it is exposed to air at 650°C for 4h (Figure 3a). In contrast, we observe that if ~ 3 nm Pt nanoparticles on SiO_2 or Al_2O_3 are physically mixed with metal-free Al-CHA crystals, and subsequently treated at 650°C in O_2 (see Scheme 2 in Figure S5), nearly full migration of the metal from the weakly interacting SiO_2 and Al_2O_3 supports to the CHA occurs, as evidenced by EDX-STEM chemical mapping of the treated Pt/SiO_2-CHA mixture (see FE-SEM and STEM images in Figure 3 and Figure S7). CeO_2 in Pt/Al_2O_3-CeO_2 catalysts have been recently suggested to play similar roles.(*16*). These results confirm that, under these conditions, volatile PtO_x species migrate over micron distances between support particles, with CHA acting as a metal trap that prevents metal sintering and, thus, prolongs the catalyst lifetime (see examples below). As expected, similar results are obtained if $Pt(NH_3)_4(NO_2)_2$ is incorporated by incipient wetness impregnation onto amorphous support (i.e. SiO_2, see experimental details in Supporting Information) and the same operations are repeated (Figure S8b, and S8c).

We have successfully synthesized sintering-resistant CHA materials containing not only Pt, but other noble metals such as Pd, or Pd-Pt mixtures, using ion-exchange followed by O_2 activation procedures. STEM images of these catalysts after calcination in air at 650°C and reduction in H_2 at 400°C show the presence of small 0.8-1.5 nm metal particles in all cases (see Figures 2b and 2c).

Thus, we conclude similar surface chemistries in all these cases: 1) small clusters form in H_2, which get encapsulated inside cages or distorted cages of the zeolite; 2) the clusters re-disperse into single noble metal atoms in O_2 at elevated temperatures, getting trapped at the Al zeolite centers; and 3) the clusters and single atoms are reversibly interconverted in H_2 and O_2, respectively. EXAFS, XANES and STEM taken at room temperature after each thermal step are consistent with these inferences for the Pt, Pd and Pt-Pd catalysts (see Figures 1 and 2 and Table 1). The structure of the mononuclear species, surrounded by 3 or 4 oxygen atoms, is not fully resolved yet, but EXAFS provides further structural information on the nature of the reduced bimetallic PtPd/CHA sample. Upon formation of small nanoparticles in H_2 at 400°C, as determined by STEM (Figure 2c), clear features of a direct Pt-Pd bond can be inferred from both the Pd K and the Pt LIII edges (Figure S9E-9H). Quantitative fitting of the data indicates that the total Pt-Me c.n. is greater than the total Pd-Me c.n., suggesting that larger nanoparticles, or their core, are slightly enriched in Pt.(*26*) Nonetheless, comparisons with previous EXAFS results on model core-shell (Pd@Pt or Pt@Pd) and well-alloyed Pt-Pd ensembles (*26*) reveals that the small Pt-Pd clusters formed inside CHA are predominantly alloyed (see SI). As occurred with the monometallic Pt/CHA and Pd/CHA counterparts, contact of the reduced bimetallic PtPd/CHA with O_2 at 500°C leads to the formation of fully segregated single Pt and Pd atoms, via oxidative fragmentation of the bimetallic nanoparticles. New ~1 nm bimetallic particles appear again in H_2 at 400°C (Figure 1 and Table 1).

As discussed above, the ultrahigh stability of Pt/CHA during oxidative-reductive cycles is striking, with potential application in the conversion of small molecules at high temperatures. The water gas shift (WGS) reaction in fuel cells is an illustrative example. Platinum nanoparticles on alumina (Al_2O_3) or on ZSM-5 are common catalysts in these processes but, unfortunately, they suffer from severe deactivation by metal sintering in the presence of strongly reducting (e.g. CO) and strong oxidizing (e.g. O_2) atmospheres at high temperatures.(*6, 27*) In this regard, the Pt/CHA catalyst shows an extremely high stability compared to Pt/Al_2O_3 when tested at temperatures higher than 350°C in the WGS reaction, where the presence of CO and steam cause the metal to aggregate on the Al_2O_3 surface, but not inside the CHA crystals (see Figure 4). Remarkably, the stability is comparable to the Pt/Al_2O_3-CeO_2 system (*16*), demonstrating that it is possible to achieve extraordinary sinter-resistant properties under severe redox stress without a reducible support (*16*), which opens a new family of materials with additional catalytic characteristics (such as Brønsted acidity, and shape-selectivity).

To summarize, the results presented here demonstrate that Al-containing CHA (Si/Al ~8) with small crystal sizes is an excellent support of noble metal species in applications where small molecules must be reacted under harsh conditions, due to its outstanding sinter-resistant characteristics. Inside CHA, Ostwald-ripening, occurring in O_2, is avoided despite the disintegration of the small metal clusters, thanks to a metal (single) atom-trapping effect. Based on these findings, we have been able to provide alternative synthesis routes for the preparation of new, highly sinter-resistant metal-encapsulated materials (including bimetallic samples), using conventional wetness impregnation methods, and solid-to-solid transformations (transport of MeO_x species from outside the CHA to its interior in O_2 at high temperatures). The metal particle encapsulation and the metal atom trapping phenomena are essential attributes of a remarkable performance in the WGS reaction when compared to other non-reducible supports.

Acknowledgements

This work has been supported by the Spanish Government-MINECO through ‘‘Severo Ochoa” (SEV 2012-0267), MAT2015-71261-R, by the European Union through ERC-AdG-2014-671093 (SynCatMatch) and by the Fundación Ramón Areces through a research contract of the “Life and Materials Science“ program. The Electron Microscopy Service of the UPV is acknowledged for their help in sample characterization. This research used beamline 9-BM and 20-ID of the Advanced Photon Source, a U.S. Department of Energy (DOE) Office of Science User Facility operated for the DOE Office of Science by Argonne National Laboratory under Contract No. DE-AC02-06CH11357. We thank Isabel Millet, Elisa García and Paul Stevens for technical assistance, and Aaron Sattler, Randall Meyer, Rob Carr, and Gary Casty for review of the manuscript and interesting scientific discussions. We appreciate the support of ExxonMobil Research and Engineering in this fundamental research area.

Figure 1. FT-EXAFS spectra of Pt, Pd, and Pt-Pd in small crystal CHA (Si/Al = 8) synthesized via ion-exchange after various sequential thermal treatments in a flow EXAFS cell under 30 ml/min of 4% H_2 or 20% O_2 at 400°C and 550°C, respectively. Table 2 shows quantitative EXAFS information upon fitting of steps 2 and 3 (1st and 2nd reduction and oxidation steps, respectively).

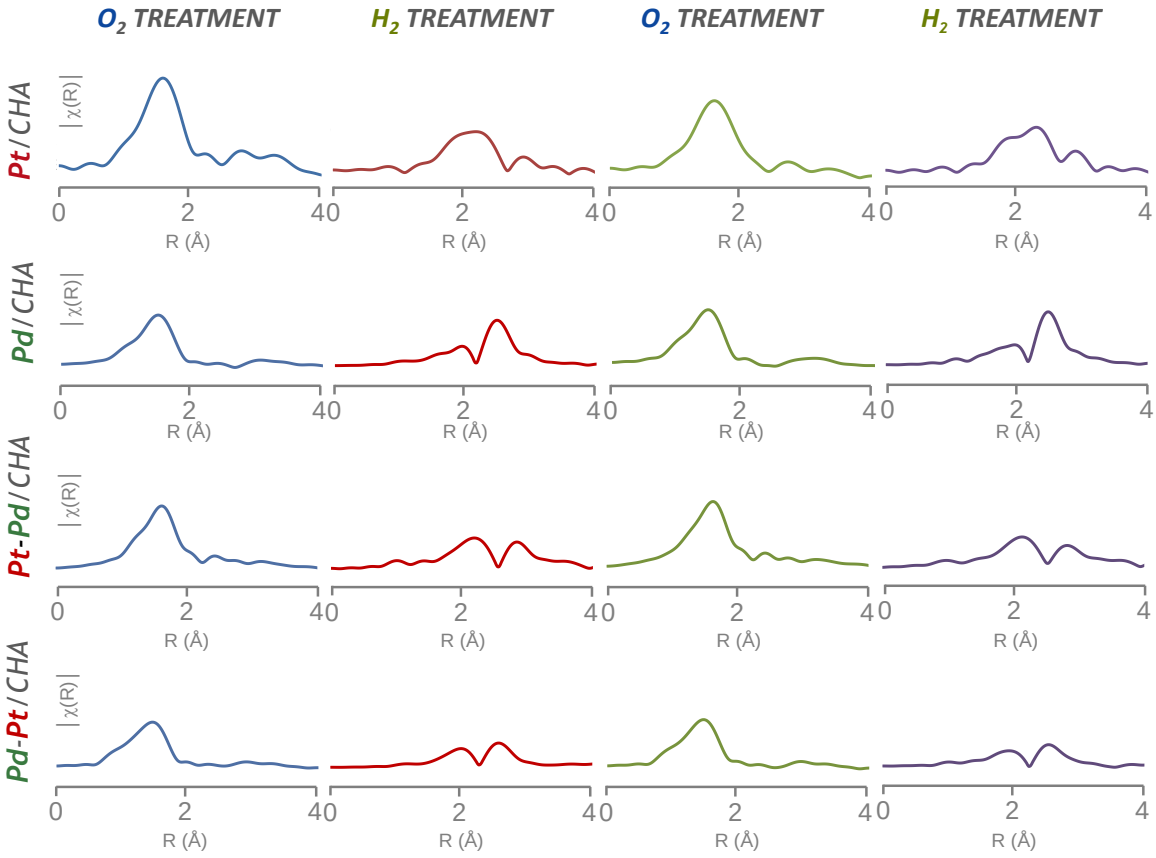

Figure 2. STEM images of the Pt/CHA-8 (a), Pd/CHA-8 (b) and PtPd/CHA-8 (c) zeolites prepared by post-synthetic metal exchange after being been treated with air at 650°C and H_2 at 400°C (O650R400) for 2 h.

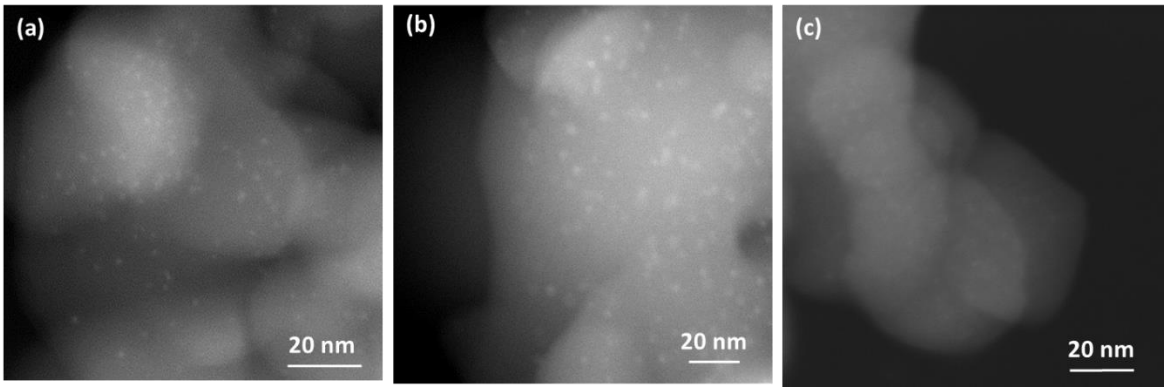

Figure 3. (a, d) FE-SEM images of Pt/SiO_2 and Pt/Al_2O_3 samples, containing initially dispersed Pt nanoparticles of ~3-5 nm, after being treated with air at 650°C; (b, e) FE-SEM images of the physical mixture of Al-CHA with Pt/SiO_2 or Pt/Al_2O_3 after being treated with air at 650°C; (c, f) STEM images of the physical mixture of Al-CHA with Pt/SiO_2 or Pt/Al_2O_3 after being treated with air at 650°C and H_2 at 400°C.

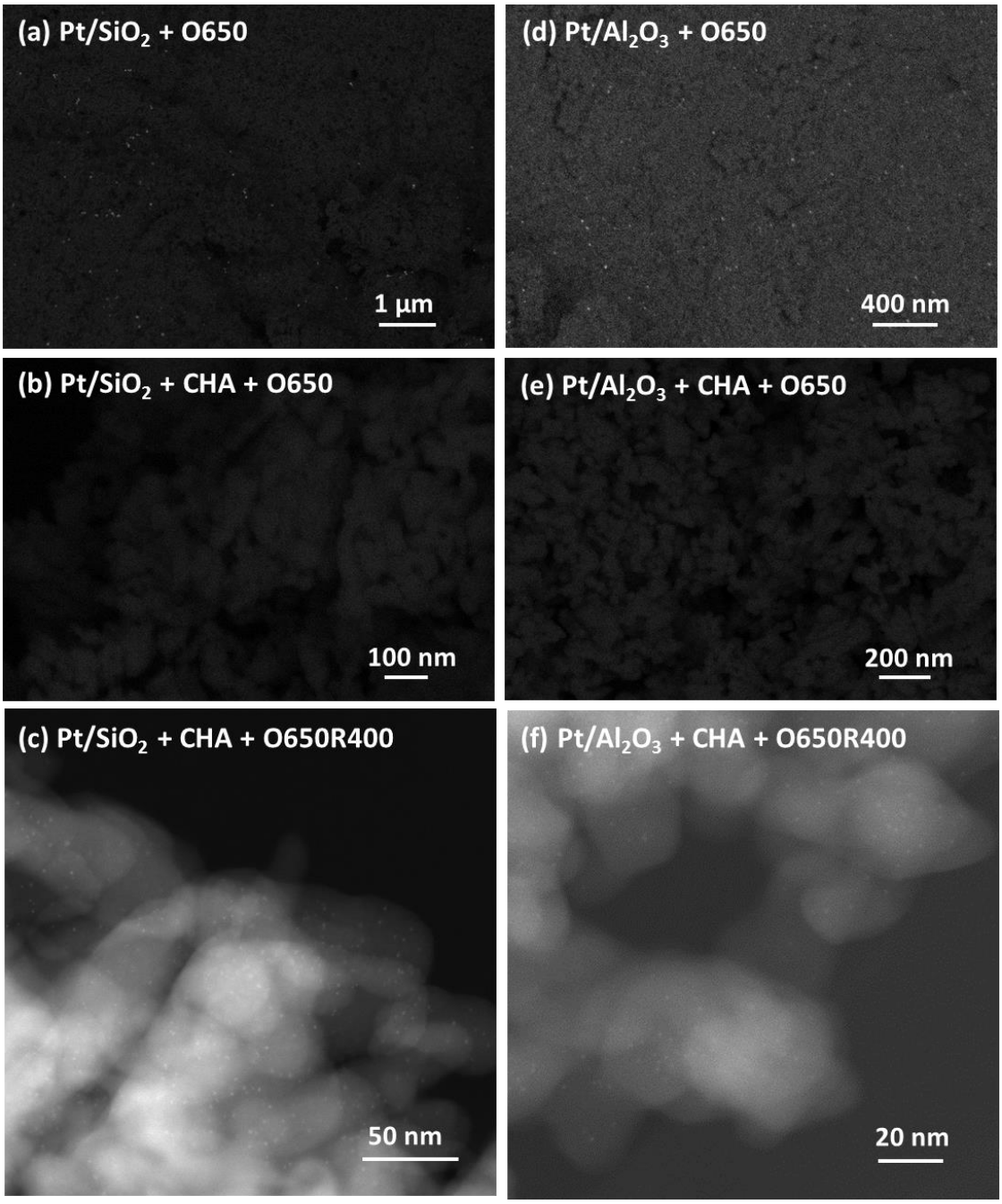

Figure 4. CO conversion at TOS (7, 14 and 21 minutes) for the Pt-CHA and Pt-Al_2O_3 catalysts at various temperatures and times on stream (Top); FESEM images of these sample after reaction. Reaction conditions: 100 ml/min; 1% CO, 2% H_2O, 200-500°C.

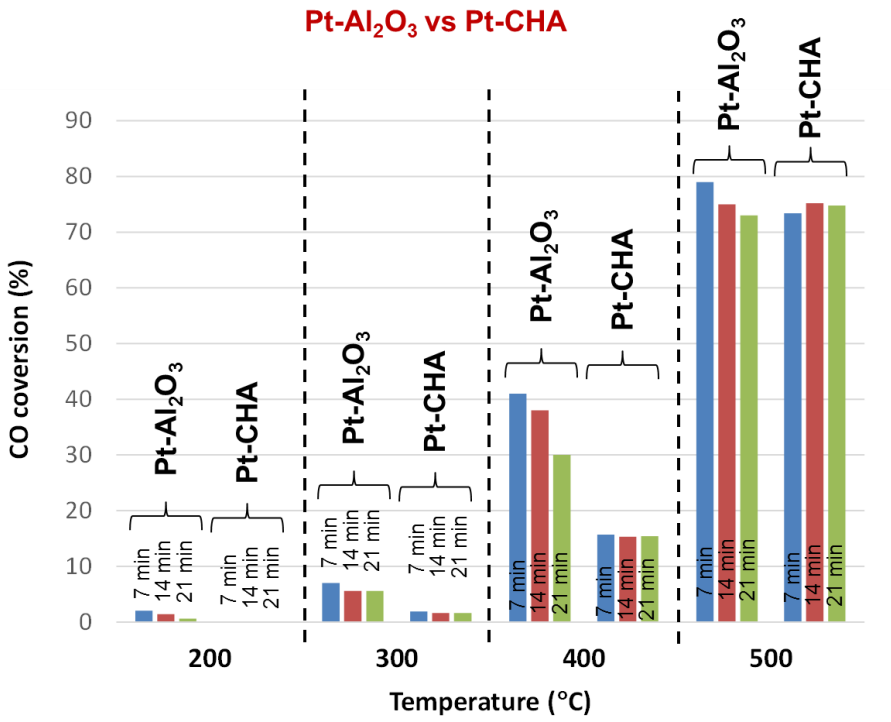

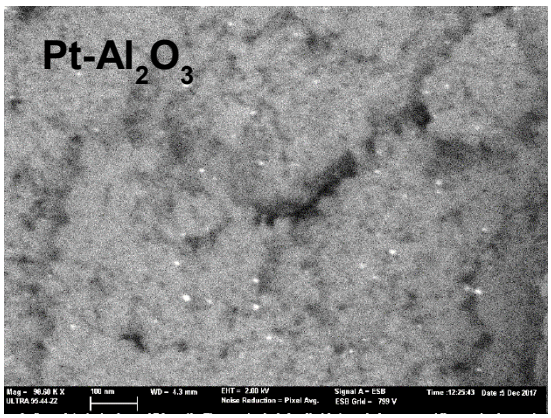

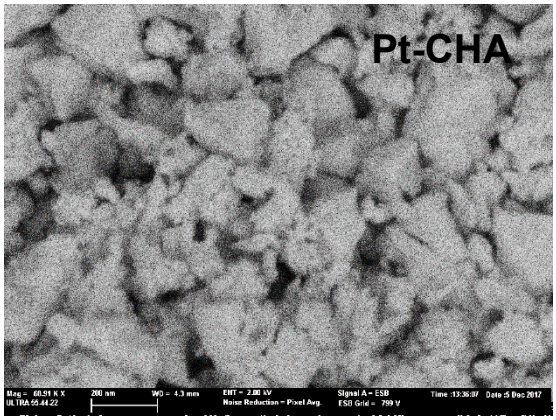

Table 1. EXAFS Data[a] at the Pt-L3 and Pd-K Edge Characterizing Pt/CHA, Pd/CHA and Pt-Pd/CHA synthesized via ion-exchange[b] after treatments in H_2 and O_2.

		H_2 (400°C)[c]				O_2 (550°C)[d]			
Sample	**Shell**	**R**	**N**	**$\Delta\sigma^2$**	**ΔE_o**	**R**	**N**	**$\Delta\sigma^2$**	**ΔE_o**
Pt/CHA	Pt-Pt	2.74	7.7	0.0051	4.7	-	-	-	-
	Pt-O	-	-	-	-	2.01	3.8	0.0025	12.5
Pd/CHA	Pd-Pd	2.73	6.5	0.0077	-6.3	-	-	-	-
	Pd-O	-	-	-	-	2.02	3.9	0.028	2.2
PtPd/CHA	Pt-Pt	2.73	7.7	0.0078	6.7	-	-	-	-
	Pt-Pd	2.74	2.5	0.0073	9.0	-	-	-	-
	Pt-O	-	-	-	-	2.01	3.4	0.0013	12.7
	Pd-Pd	2.75	2.7	0.0072	-6.3	-	-	-	-
	Pd-Pt	2.74	3.2	0.0073	-5.3	-	-	-	-
	Pd-O	-	-	-	-	2.02	3.8	0.0029	-1.4

[a]Notation: N, coordination number; R, distance between absorber and backscatterer atoms; $\Delta\sigma^2$, Debye−Waller factor; ΔE_0, inner potential correction. Error bounds (accuracies) characterizing the structural parameters obtained by EXAFS spectroscopy are estimated to be as follows: coordination number N, ∼20%; distance R, ∼0.02; Debye−Waller factor $\Delta\sigma^2$, ∼20%; and inner potential correction ΔE0, ∼20%. Fitting plots provided in the SI; [b] See SI for experimental details; [c] Samples were first calcined in 10 % O_2 at 550°C, and then reduced with 50 sccm of 4 % H_2 at 1 atm for 2 h; [d] Samples treated according to *c* were further treated with 50 sccm of 20 % O_2 at 1 atm for 2h.

Table 2. ICP analyses of the different metal-containing catalysts.

Entry	*Sample*	*Initial Preparation method*	*Si/Al*	*Pt (%wt)*	*Pd (%wt)*
(1)	Pt/CHA_op	One-pot [Pt-Thiolsilane]	7.9	0.21	---
(2)	CHA-8	Metal-free	8.8	---	---
(3)	CHA-12	Metal-free	12.3	---	---
(4)	CHA-25	Metal-free	32.0	---	---
(5)	Pt/CHA-8_exc	Metal-exchange [$Pt(NH_4)^{2+}$]	9.0	0.31	---
(6)	Pt/CHA-12_exc	Metal-exchange [$Pt(NH_4)^{2+}$]	12.5	0.32	---
(7)	Pt/CHA-25_exc	Metal-exchange [$Pt(NH_4)^{2+}$]	30.3	0.15	---
(8)	Pd/CHA-8_exc	Metal-exchange [$Pd(NH_4)^{2+}$]	8.8	---	0.33
(9)	PtPd/CHA-8_exc	Metal-exchange [$Pt(NH_4)^{2+}$+ $Pd(NH_4)^{2+}$]	8.8	0.17	0.09

Supporting Information

1.- Experimental

1.1.- Synthesis of the OSDA

- Synthesis of N,N,N-trimethyl-1-adamantammonium (TMADA)

29.6 g of 1-Adamantamine (Sigma-Aldrich) and 64 g of potassium carbonate (Sigma-Aldrich) were mixed with 320 ml of chloroform. At this point, 75 g of methyl iodide was added dropwise while the reaction was stirred in an ice bath. The reaction was maintained during 5 days under agitation at room temperature. The mixture was filtered and washed with diethyl ether, and the resultant solid further extracted with chloroform. The final product was N,N,N-trimethyl-1-adamantammonium iodide. This iodide salt was anion exchanged using an ion exchange resin achieving the hydroxide form.

1.2.- Synthesis of metal-containing CHA zeolites

- One-pot synthesis of the Pt-containing CHA zeolite (Pt/CHA_op)

640 mg of sodium hydroxide (99%, Sigma-Aldrich) was dissolved in 6.9 g of water. Then, 68 mg of a 10%wt aqueous solution of chloroplatinic acid ($H_2PtCl_6.6H_2O$, Sigma-Aldrich) and 52 mg of (3-mercaptopropyl)trimethoxysilane (TMSH, 95%, Sigma-Aldrich) were added to the above solution, and the mixture stirred for 30 minutes. Afterwards, 9.66 g of an aqueous solution of N,N,N-trimethyl-1-adamantammonium hydroxide (TMAdA, 17.5%wt) was added and maintained under stirring during 15 minutes. At that time, 235 mg of aluminum hydroxide (66%wt, Sigma-Aldrich) was added, and the resultant mixture kept under stirring at 80°C for 30 minutes. Finally, 6 g of colloidal silica (Ludox AS40, 40%wt, Aldrich) was introduced in the synthesis mixture, and maintained under stirring at 80°C for 30 minutes. The resultant gel was allowed to reach the desired silica to water ratio by evaporation under stirring. The final gel composition was SiO_2 : 0.038 Al_2O_3 : 0.00033 Pt : 0.005 TMSH : 0.2 TMAdA : 0.4 NaOH : 20 H_2O.

The gel was transferred to an autoclave with a Teflon liner, and heated at 160°C for 2 days under dynamic conditions. The sample after the hydrothermal crystallization was filtered and washed with abundant distilled water, and finally dried at 100°C. Calcination of the solid samples to remove the organic molecules occluded within the crystals was performed in air at 580°C for 6 h.

- Synthesis of the metal-free CHA zeolite with a Si/Al molar ratio of 8 (CHA-8)

640 mg of sodium hydroxide (99%, Sigma-Aldrich) was dissolved in 18.37 g of an aqueous solution of N,N,N-trimethyl-1-adamantammonium hydroxide (TMAdA, 9.2%wt) and maintained under stirring during 15 minutes. At that time, 234 mg of aluminum hydroxide (66%wt, Sigma-Aldrich) was added, and the resultant mixture kept under stirring at 80°C for 30 minutes. Finally, 6 g of colloidal silica (Ludox AS40, 40%wt, Aldrich) was introduced in the synthesis mixture, and maintained under stirring at 80°C for 30 minutes. The resultant gel was allowed to reach the desired silica to water ratio by evaporation under stirring. The final gel composition was SiO_2 : 0.038 Al_2O_3 : 0.2 TMAdA : 0.4 NaOH : 20 H_2O.

The gel was transferred to an autoclave with a Teflon liner, and heated at 160°C for 2 days under dynamic conditions. The sample after the hydrothermal crystallization was filtered and washed with abundant distilled water, and finally dried at 100°C. Calcination of the solid samples to remove the organic molecules occluded within the crystals was performed in air at 580°C for 6 h.

- Synthesis of the metal-free CHA zeolite with a Si/Al molar ratio of 12 (CHA-12)

320 mg of sodium hydroxide (99%, Sigma-Aldrich) was dissolved in 18.37 g of an aqueous solution of N,N,N-trimethyl-1-adamantammonium hydroxide (TMAdA, 9.2%wt) and maintained under stirring during 15 minutes. At that time, 234 mg of aluminum hydroxide (66%wt, Sigma-Aldrich) was added, and the resultant mixture kept under stirring at 80°C for 30 minutes. Finally, 6 g of colloidal silica (Ludox AS40, 40%wt, Aldrich) was introduced in the synthesis mixture, and maintained under stirring at 80°C for 30 minutes. The resultant gel was allowed to reach the desired silica to water ratio by evaporation under stirring. The final gel composition was SiO_2 : 0.038 Al_2O_3 : 0.2 TMAdA : 0.2 NaOH : 20 H_2O.

The gel was transferred to an autoclave with a Teflon liner, and heated at 160°C for 2 days under dynamic conditions. The sample after the hydrothermal crystallization was filtered and washed with abundant distilled water, and finally dried at 100°C. Calcination of the solid samples to remove the organic molecules occluded within the crystals was performed in air at 580°C for 6 h.

- Synthesis of the metal-free CHA zeolite with a Si/Al molar ratio of 25 (CHA-25)

22,96 g of an aqueous solution of N,N,N-trimethyl-1-adamantammonium hydroxide (TMAdA, 9.2%wt) was mixed with 88 mg of aluminum hydroxide (66%wt, Sigma-Aldrich) and 3,76 g of colloidal silica (Ludox AS40, 40%wt, Aldrich), and maintained under stirring at 80°C for 30 minutes. Then, 3,7 g of an a 10%wt solution of NH_4F (Sigma-Aldrich) was added, and the resultant mixture gel

was allowed to reach the desired silica to water ratio by evaporation under stirring. The final gel composition was SiO_2 : 0.023 Al_2O_3 : 0.4 TMAdA : 0.4 NH_4OH : 10 H_2O.

The gel was transferred to an autoclave with a Teflon liner, and heated at 160°C for 5 days under dynamic conditions. The sample after the hydrothermal crystallization was filtered and washed with abundant distilled water, and finally dried at 100°C. Calcination of the solid samples to remove the organic molecules occluded within the crystals was performed in air at 580°C for 6 h.

- Post-synthetic metal-exchange procedure to prepare Pt/CHA-8_exc, Pd/CHA-8_exc, PtPd/CHA-8_exc, Pt/CHA-12_exc and Pt/CHA-25_exc

The procedure employed to attempt the introduction of ~0.3%wt of metal species within the different small-pore zeolites by post-synthetic cationic is the following: first, the an aqueous solution of the required metal source [$Pt(NH_3)(NO_3)_2$ and/or $Pd(NH_3)(NO_3)_2$] is prepared, followed by the addition of zeolite crystals to the above aqueous solution under agitation (liquid/solid ratio of 10wt/wt). The mixture is maintained under stirring at room temperature overnight. After this period, the mixture is filtered and washed with abundant water, and the resultant solids calcined at 650°C in air for 4 hours. Finally, the resultant metal-containing zeolites are treated with H_2 at 400°C for 2 h.

- Post-synthetic incipient wetness impregnation procedure to prepare a Pt-containing CHA zeolite with Pt nanoparticles of ~3 nm deposited on the external surface of the CHA crystals

300 mg of CHA-8 was impregnated with 0.665 g of a ~3 nm Pt nanoparticle dispersion (1,000 ppm in H_2O, 99.99% trace metals basis, Sigma-Aldrich). The Pt-containing CHA zeolite was dried overnight at room temperature and, afterwards, at 100°C for 2 hours. The Pt content in the final mixture was measured by ICP, revealing a %wtPt content of 0.22. The resultant solid was treated with O_2 at 650°C (see FE-SEM image in Figure S6b) and, subsequently, treated with H_2 at 400°C (see FE-SEM image in Figure S6c).

- Procedure to prepare a physical mixture of a Pt-containing amorphous SiO_2 and a metal-free CHA zeolite using Pt nanoparticles (~3 nm) as Pt precursor [3nm Pt/SiO_2+CHA]

1 g of Aerosil (XXXX) was impregnated with 3 g of a ~3 nm Pt nanoparticle dispersion (1,000 ppm in H_2O, 99.99% trace metals basis, Sigma-Aldrich). The Pt-containing silica was dried overnight at room temperature and, afterwards, at 100°C for 2 hours. 200 mg of the resultant Pt-SiO_2 was physically mixed with 200 mg of the calcined metal-free CHA-8 sample. The Pt content in the final mixture was

measured by ICP, revealing a %wtPt content of 0.15. The resultant solid was treated with O_2 at 650°C (see FE-SEM image in Figure 3b) and, subsequently, treated with H_2 at 400°C (see FE-SEM image in Figure 3c).

- Procedure to prepare a physical mixture of a Pt-containing Al_2O_3 and a metal-free CHA zeolite using a commercially available Pt/Al_2O_3 precursor [5nm Pt/Al_2O_3+CHA]

100 mg of a commercially available Pt/Al_2O_3 (1%wt Pt, XXXX) was physically mixed with 400 mg of the calcined metal-free CHA-8 sample. The Pt content in the final mixture was measured by ICP, revealing a %wtPt content of 0.19. The mixture was treated with O_2 at 650°C (see FE-SEM image in Figure 3e) and, subsequently, treated with H_2 at 400°C (see FE-SEM image in Figure 3f).

- Procedure to prepare a physical mixture of a Pt-containing amorphous SiO_2 and a metal-free CHA zeolite using $[Pt(NH_3)_4]^{2+}$ as Pt precursor [Pt/SiO_2+CHA]

1 g of Aerosil (XXXX) was impregnated with 3 g of an aqueous solution of $Pt(NH_3)(NO_3)_2$ [6 mg of $Pt(NH_3)(NO_3)_2$, Sigma-Aldrich, in 3 g of water]. The Pt-containing silica was dried overnight at room temperature and, afterwards, at 100°C for 2 hours. 200 mg of the resultant Pt-SiO_2 was physically mixed with 200 mg of the calcined metal-free CHA-8 sample. The Pt content in the final mixture was measured by ICP, revealing a %wtPt content of 0.16. The resultant solid was treated with O_2 at 650°C (see FE-SEM image in Figure S8b) and, subsequently, treated with H_2 at 400°C (see FE-SEM image in Figure S8c).

1.3.- Characterization

Powder X-ray diffraction (PXRD) measurements were performed with a multisample Philips X'Pert diffractometer equipped with a graphite monochromator, operating at 40 kV and 35 mA, and using Cu Kα radiation (λ = 0,1542 nm). The chemical analyses were carried out in a Varian 715-ES ICP-Optical Emission spectrometer, after solid dissolution in HNO_3/HCl/HF aqueous solution.

The morphology of the samples was studied by field emission scanning electron microscopy (FESEM) using a ZEISS Ultra-55 microscope, and by field emission transmission electron microscopy (TEM) using a JEM 2100F microscope. The TEM imaging was done using a Philips CM200 TEM/STEM operated at 200kV. The STEM images were collected with a High Angle Annular Dark Field detector. Materials were prepared for analysis in the TEM by crushing them into fines (< ~1000 nm thick) using an agate mortar and pestle. The fines were dusted onto 200 mesh, holey carbon coated grids.

1.4.- EXAFS measurements

XAFS experiments were performed at beamline 9-BN (Pt/CHA) and 20-ID (Pd/CHA and Pt-Pd/CHA) at Advanced Photon Source (APS) at the Argonne National Laboratory. Data were collected in fluorescence mode using a XAFS cell that also acted as a flow reactor. The samples were scanned in the presence of flowing gases (30-50 sccm) at variable temperatures. 4 % H_2 (in He) was used to perform the in situ reductions, whereas 20 % O_2 (in He) was used for the in situ oxidation treatments. The storage ring electron energy and ring currents were 7.0 GeV and 105 mA, respectively. A water-cooled Si(111) monochromator was used to scan X-ray energy from -250 to 1000 eV relative to Pt L3 edge (11564 eV). Each sample (~20 mg) was pressed as a thin wafer inside an air tight EXAFS cell, using a multi-ion Ge detector to collect data in fluorescence mode. Transmission XAFS measurements were carried out simultaneously with the pure Pt and Pd metals measured in reference mode for X-ray energy calibration and data alignment. Data processing and analysis were performed using the IFEFFIT pack-age.(*28*) EXAFS analysis was done model-independently, and the results were not biased in favor of any assumed model about the short-range order of elements in these samples. Specifically, multiple-edge (Pt L3) analysis was employed by fitting theoretical FEFF6 calculations (*29*) to the experimental EXAFS data in R space. The values of passive electron reduction factor, S_0^2, were obtained from fits to their corresponding standards, and were fixed in the analysis of the samples. The parameters describing electronic properties (e.g., correction to the photoelectron energy origin) and local structural environment (coordination numbers N, bond length R, and their mean-squared relative derivation, σ^2) around absorbing atoms were varied during fitting. In addition, the physically reasonable constraints between the fitting parameters for the first nearest neighbor (1NN) pairs were applied.

1.5.- Catalytic tests

- Ethylene/propylene hydrogenation reactions

In a typical experiment, 40 mg of the Pt/CHA-8_exc (0.31 wt % Pt) catalysts was mixed with 1 g of neutral silica (silica gel, Davisil Grade 640, 35- 60 mesh) and loaded in a conventional tubular plug-flow reactor (ID = 6/16 inches 9.53 mm). High purity hydrogen, ethylene, propylene, and nitrogen were used for the experiments, with flow rates regulated by standard mass flow controllers. Prior to the hydrogenation experiment, the catalyst was reduced in situ in flow of hydrogen (50 ml/min) at 400°C for 4 h. The reactor was then cooled down to the selected reaction temperature (80°C). With the catalyst bed at 80°C, the reaction mixture was flowed at atmospheric pressure: 4 ml/min

of alkene (ethylene or propylene); 20 ml/min of H_2; and 100 ml/min of N_2. The downstream reaction effluents were analyzed by gas chromatography. For identification purposes, the position of the various reactants and products within the gas chromatogram were compared with standards commercially available. Conversions and selectivity were calculated from the corresponding GC areas.

- WGS reaction

In a typical experiment, 120 mg of the reduced Pt/CHA-8_exc (0.31 wt % Pt) or 40 mg of the as-received Pt/Al_2O_3 (1 wt % Pt) catalysts were mixed with 0.5 g of silicon carbide (Fisher Chemical) and loaded in a conventional tubular plug-flow quartz reactor (ID = 9 mm). The reactor was heated at 200°C passing a flow of N_2 through the catalyst (90 ml/min). With the catalyst bed at 200°C, the reaction mixture was flowed at atmospheric pressure: 100 ml/min, containing 1% CO, 2%H_2O, balanced in N_2. The reaction temperature was varied from 200 to 500°C. The catalytic tests have been performed first at the lowest reaction temperature (200°C) and, later, the temperature was increased under inert conditions up to the following temperature to be studied (i.e. 300, 400 and 500°C), where the catalytic behavior will be evaluated at that temperature. The downstream reaction effluents were analyzed continuously by gas chromatography. Conversions and selectivity were calculated from the corresponding GC areas.

Figure S1. STEM image of the Pt/CHA zeolite synthesized by one-pot method after being treated with air at 650°C and H_2 at 400°C for 2 h (a) and after being treated again with air at 500°C for 2 h (b).

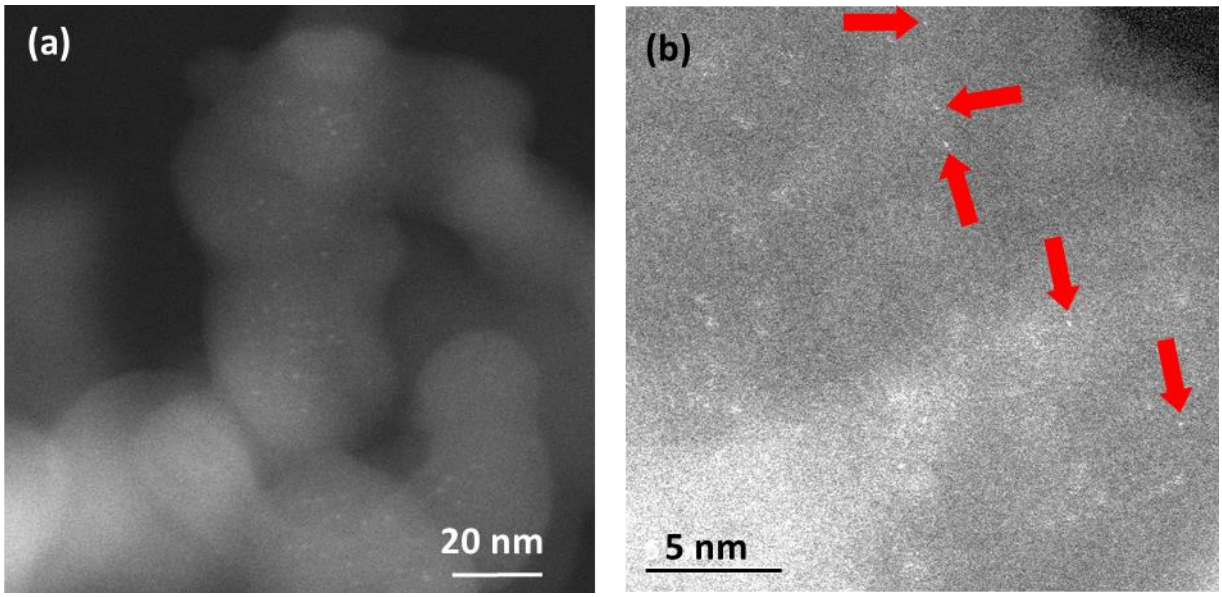

Figure S2. TEM of Pt nanoparticles in a small pore CHA (left), and in a conventional ZSM-5 (CBV2314, right) formed by ion-exchange pf $Pt(NH_3)_4(NO_2)_2$ and after the following sequence of treatments: O_2 at 650°C, H_2 at 400°C, O_2 at 650°C, and H_2 at 400°C.

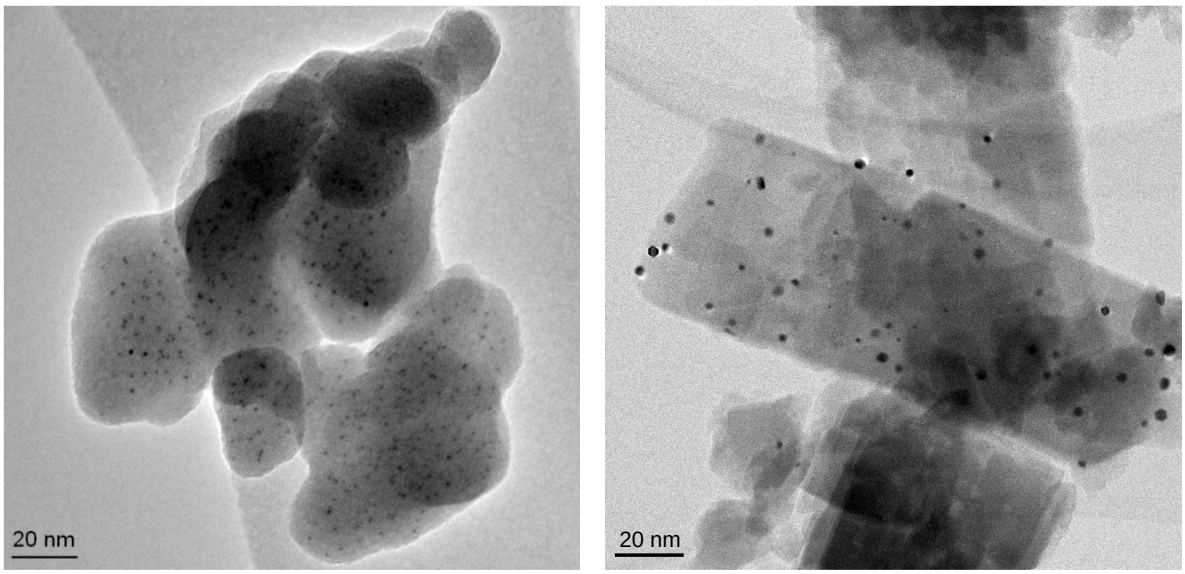

Figure S3. FE-SEM images of the metal-free CHA zeolites synthesized with different Si/Al molar ratios (left) and after introducing 0.3%wt of Pt by a post-synthetic metal-exchange procedure and being calcined in air at 650°C (right).

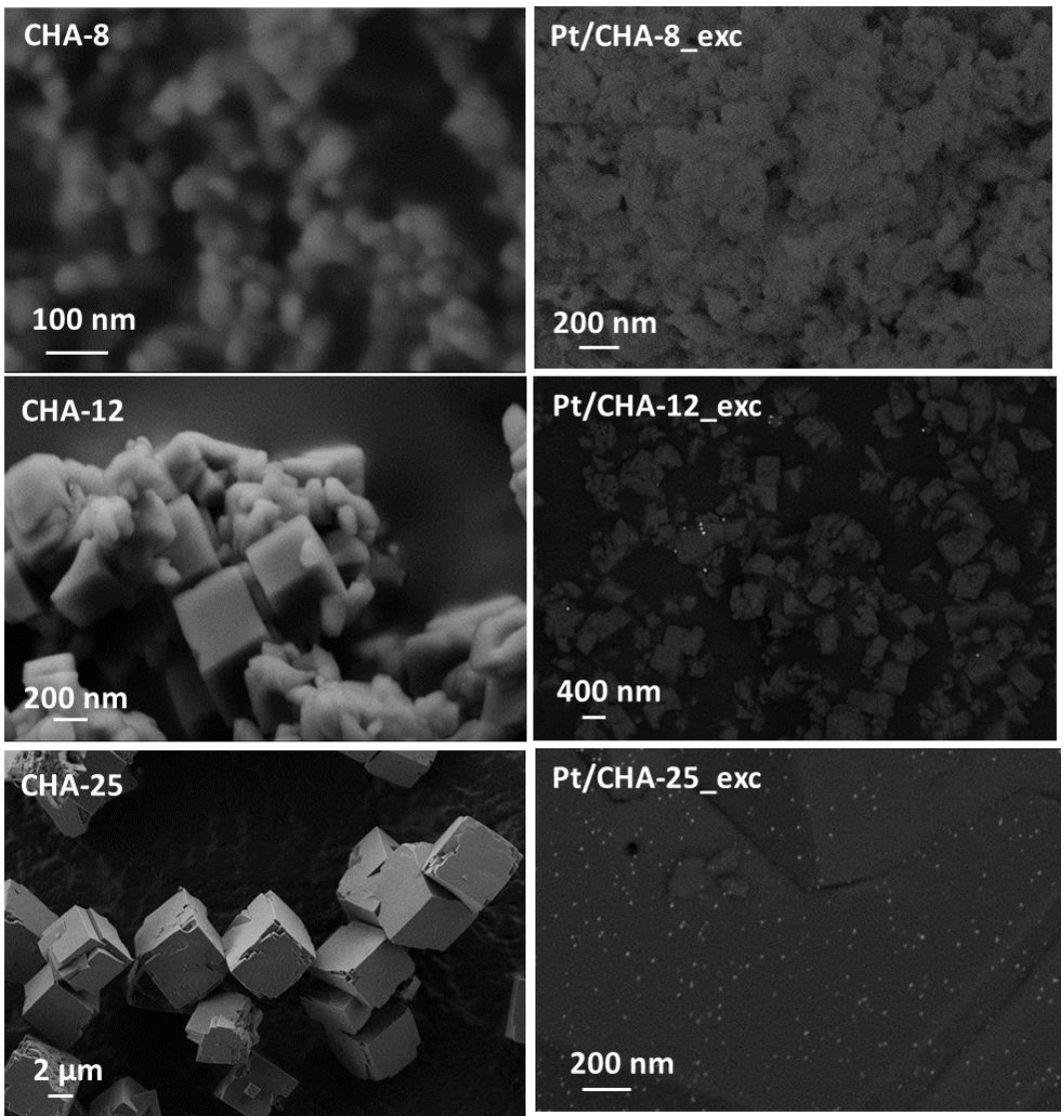

Figure S4. Hydrogenation of ethylene and propylene using 0.8 wt % Pt/SiO_2, 0.2 wt % Pt/CHA (direct synthesis method), and 0.2 wt % Pt/CHA-IE (ion-exchanged). Reaction feed: H_2 (20 sccm), alkene (4 sccm), and N2 (100 sccm). Reaction temperature: 80 °C.

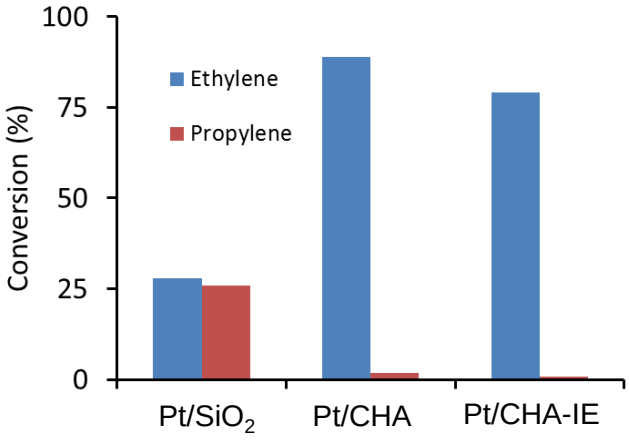

Figure S5. (Scheme 1) Scheme proposed for the atom trapping methodology when ~3 nm Pt nanoparticles are deposited on the external surface of Al-CHA crystals ; (Scheme 2) Scheme proposed for the atom trapping methodology when the Al-containing CHA is mixed with a Pt-containing SiO_2 or Al_2O_3 support.

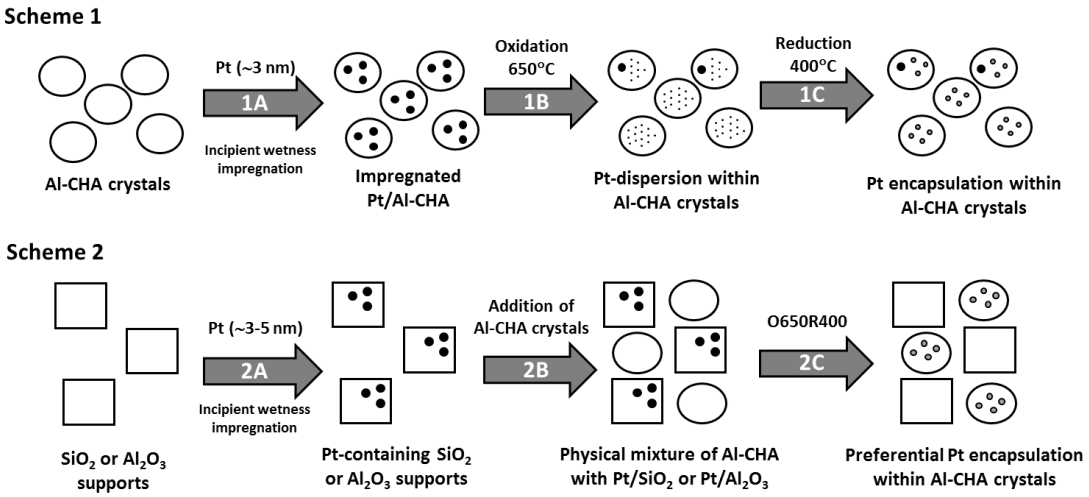

Figure S6. STEM images for the Pt/CHA zeolite containing initially deposited ~3nm Pt nanoparticles (a), after being treated with air at 650°C (b) and after being treated with air at 650°C and H_2 at 400°C (c).

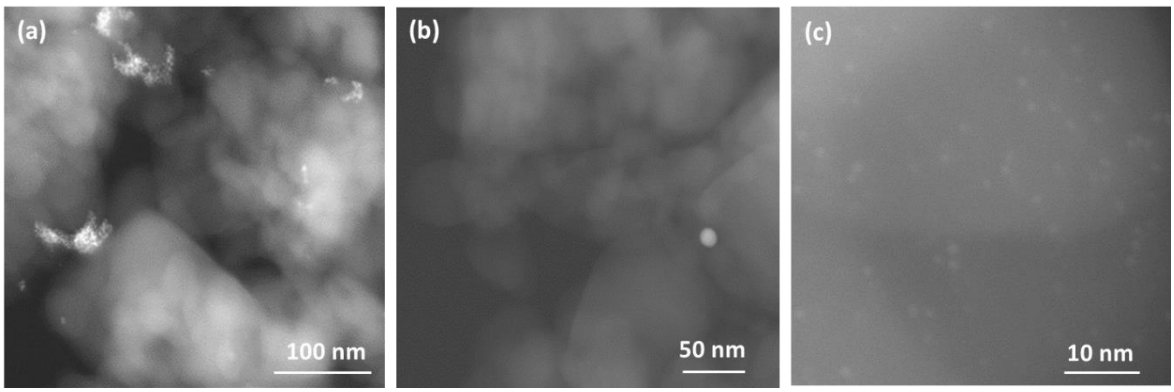

Figure S7. STEM image (a) and element mapping distribution of silicon (b) and aluminum (c) for the physical mixture of Al-CHA with Pt/SiO_2 after being treated with air at 650°C and H_2 at 400°C.

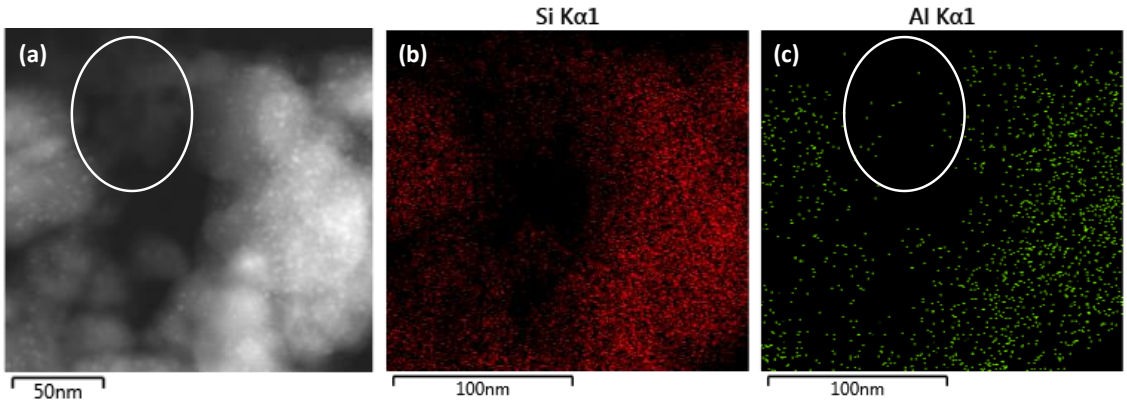

Figure S8. (a) FE-SEM image of the Pt-containing SiO_2 sample, initially prepared by incipient wetness impregnation of Aerosil with $Pt(NH_3)^{2+}$, after being treated with air at 650°C; (b) FE-SEM image of the physical mixture of Al-CHA and Pt/SiO_2 after being treated with air at 650°C; (c) STEM image of the physical mixture of Al-CHA and Pt/SiO_2 after being treated with air at 650°C and H_2 at 400°C.

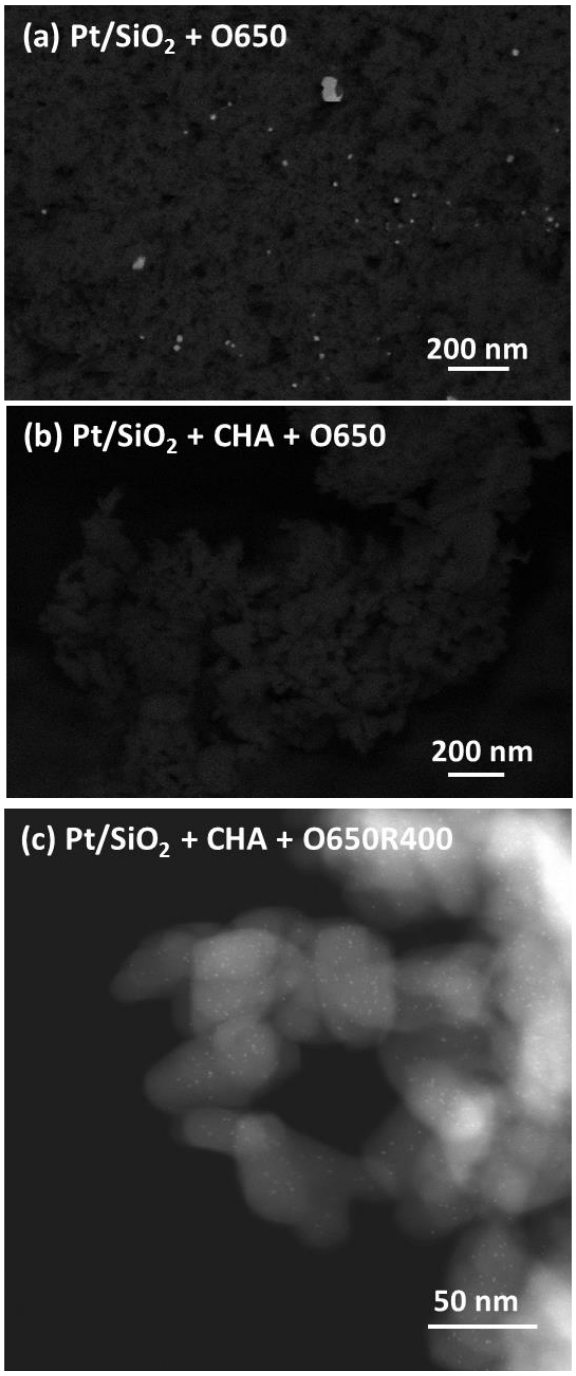

Figures S9. EXAFS data and fittings.

S9A) Pt on small crystal CHA made via ion-exchange after calcination in 10 % O_2 at 550°C and subsequent reduction in 4 % H_2 at 400°C.

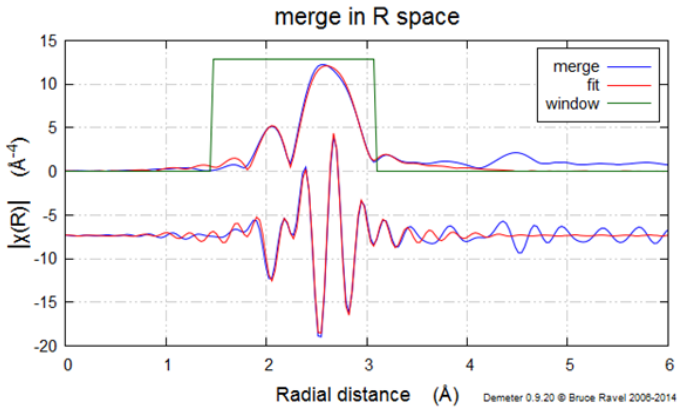

S9B) Pt on small crystal CHA made via ion-exchange after oxidation in 10 % O_2 at 550°C, subsequent reduction in 4 % H_2 at 400°C, and subsequent oxidation in 10 % O_2 at 550°C.

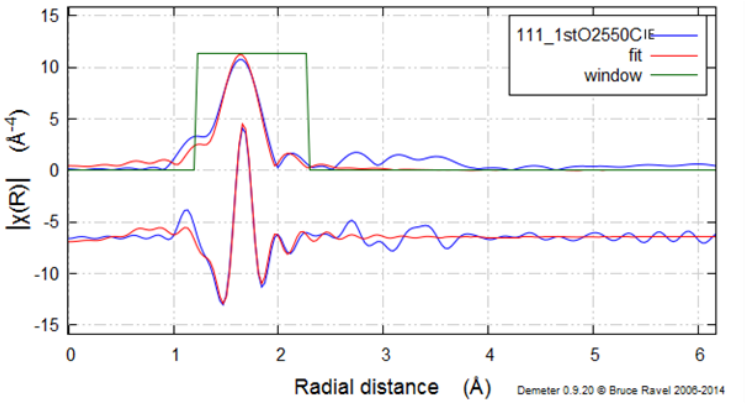

S9C) Pd on small crystal CHA made via ion-exchange after oxidation in 10 % O_2 at 550°C, subsequent reduction in 4 % H_2 at 400°C.

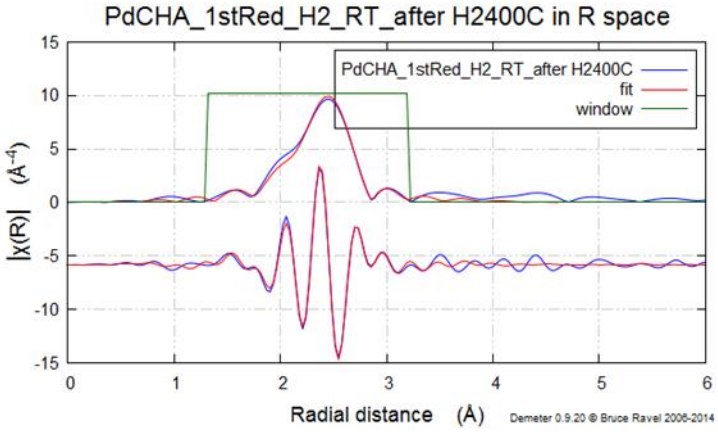

S9D) Pd on small crystal CHA made via ion-exchange after oxidation in 10 % O_2 at 550°C, subsequent reduction in 4 % H_2 at 400°C, and subsequent oxidation in 10 % O_2 at 550°C.

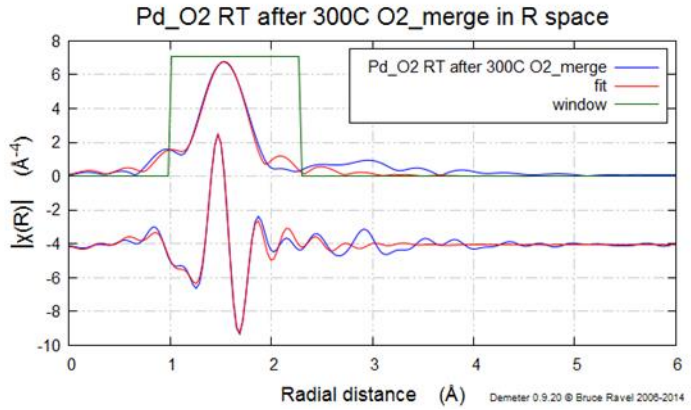

S9E) Bimetallic Pt and Pd on small crystal CHA made via ion-exchange after oxidation in 10 % O_2 at 550°C, and subsequent reduction in 4 % H_2 at 400°C (Pt Edge).

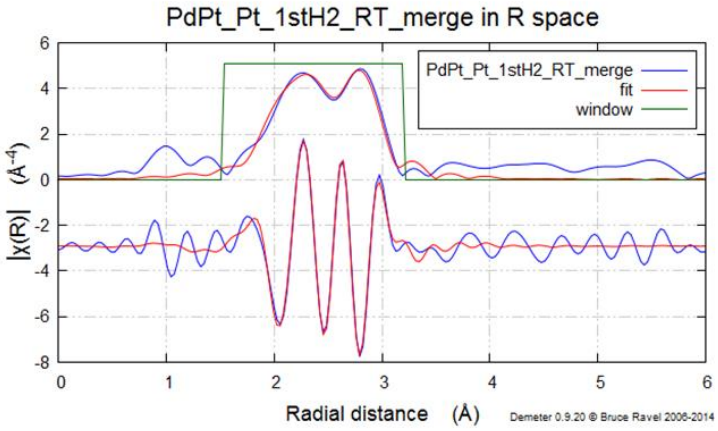

S9F) Bimetallic Pt and Pd on small crystal CHA made via ion-exchange after oxidation in 10 % O_2 at 550°C, and subsequent reduction in 4 % H_2 at 400°C (Pd Edge).

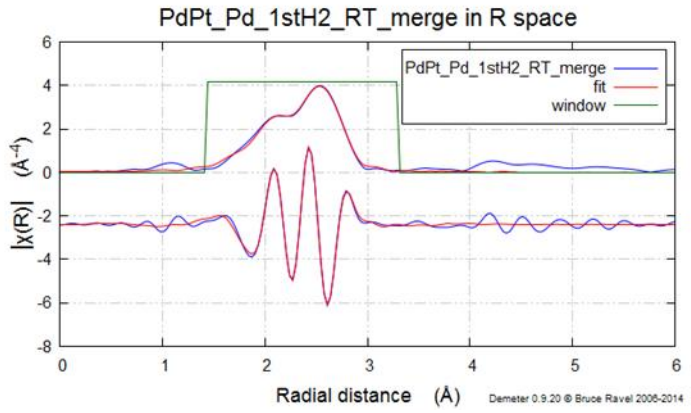

S9G) Bimetallic Pt and Pd on small crystal CHA made via ion-exchange after oxidation in 10 % O_2 at 550°C, subsequent reduction in 4 % H_2 at 400°C, and subsequent oxidation in 10 % O_2 at 550°C (Pt Edge).

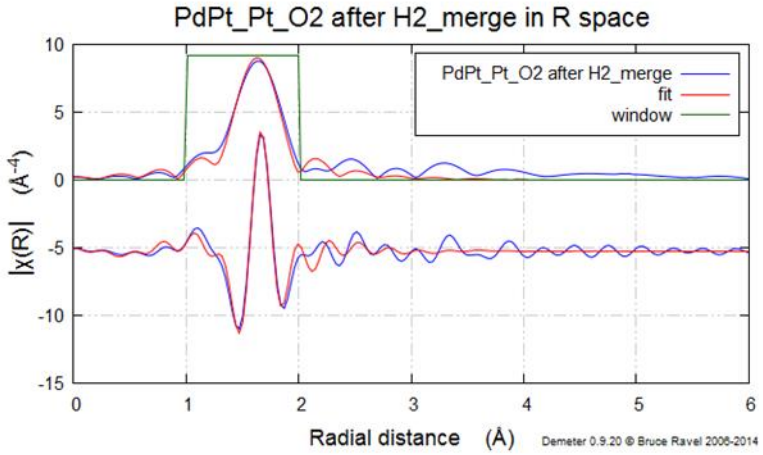

S9H) Bimetallic Pt and Pd on small crystal CHA made via ion-exchange after oxidation in 10 % O_2 at 550°C, subsequent reduction in 4 % H_2 at 400°C, and subsequent oxidation in 10 % O_2 at 550°C (Pd Edge).

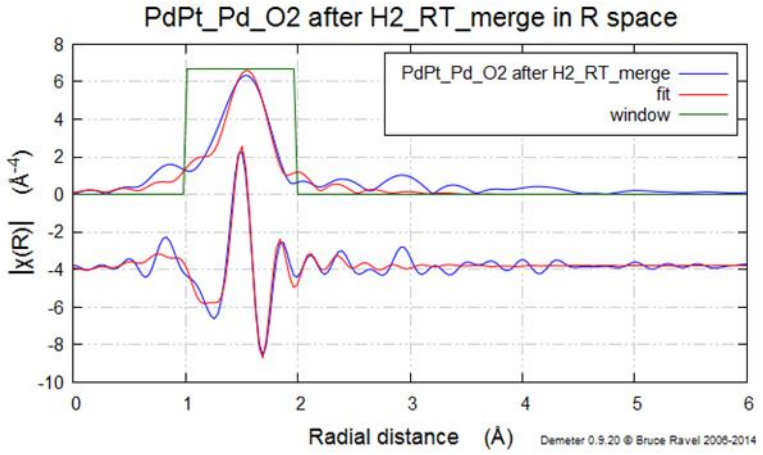

Figure S10. CO conversion at TOS (7, 14 and 21 minutes) for the Pt-CHA and Pt-Al_2O_3 catalysts (Top), and for the Pt-CHA catalyst after two full reaction cycles (Bottom) (Reaction conditions: 100 ml/min; 1% CO, 2% H_2O, 200-500°C).

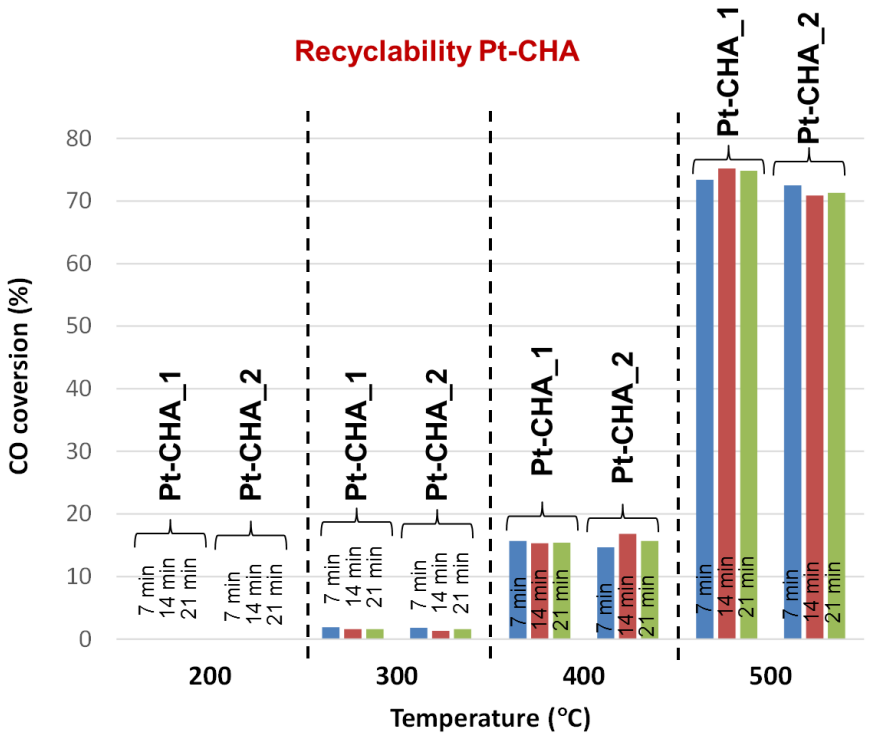

Figure S11. PXRD patterns of the metal-free CHA zeolites synthesized with different Si/Al molar ratios.

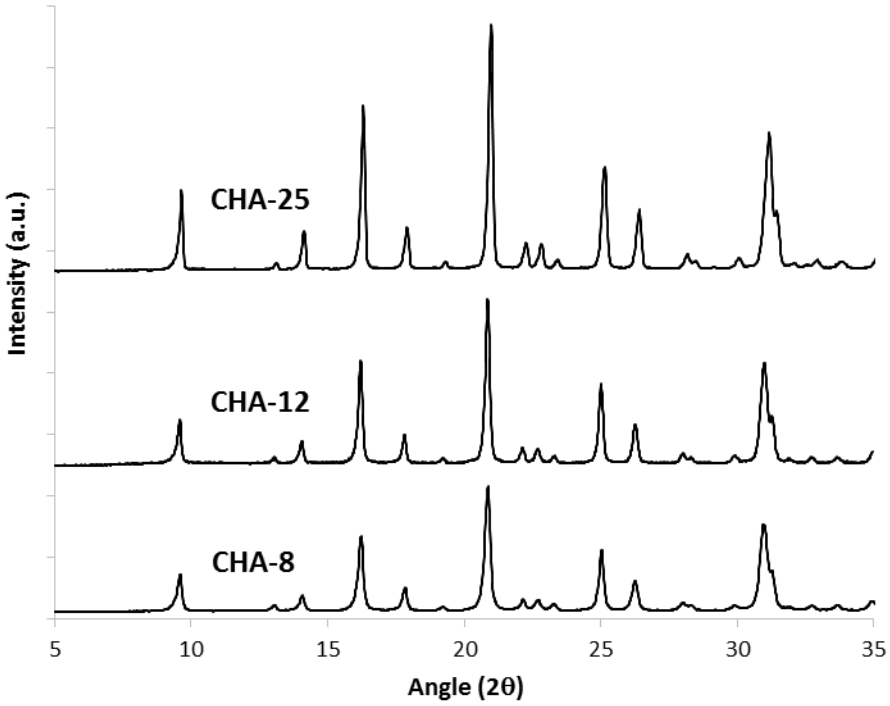

Table S1. EXAFS Data[a] at the Pt-L3 Edge Characterizing the Pt/CHA zeolite synthesized via one-pot methods (Pt/CHA_op)[b] after treatments in H_2 and O_2.

Entry	Contribution	N	R (Å)	$\Delta\sigma^2$ (Å^2)	ΔE_o (eV)
1[c]	Pt-S	3.78	2.33	0.0039	7.71
2[d]	Pt-O	3.22	2.01	0.0016	12.4
3[e]	Pt-Pt	7.36	2.74	0.0580	5.83
4[f]	Pt-O	2.71	2.02	0.0034	8.36
5[g]	Pt-Pt	6.48	2.73	0.0071	5.34

[a] Notation: N, coordination number; R, distance between absorber and backscatterer atoms; $\Delta\sigma^2$, Debye−Waller factor; ΔE_0, inner potential correction. Error bounds (accuracies) characterizing the structural parameters obtained by EXAFS spectroscopy are estimated to be as follows: coordination number N, ∼20%; distance R, ∼0.02; Debye−Waller factor $\Delta\sigma^2$, ∼20%; and inner potential correction ΔE0, ∼20%

[b] See SI for experimental details

[c] Sample as-made; spectra taken in He at 25°C.

[d] Sample in Entry 1 after *ex situ* calcination in air at 550°C for 2 h; spectra taken in air at 25°C.

[e] Sample in Entry 2 after subsequent *in situ* reduction in 4 % H_2 (balance, He) at 400°C for 1h; spectra taken in H_2 at 25°C

[f] Sample in Entry 3 after subsequent *in situ* calcination in 20 % O_2 (balance, He) at 500°C for 1h; spectra taken in air at 25°C

[g] Sample in Entry 4 after subsequent *in situ* reduction in 4 % H_2 (balance, He) at 500°C for 1h; spectra taken in air at 25°C

References:

1. J. Weitkamp, Catalytic Hydrocracking-Mechanisms and Versatility of the Process. *ChemCatChem* **4**, 292-306 (2012).
2. S. Sengodan *et al.*, Advances in reforming and partial oxidation of hydrocarbons for hydrogen production and fuel cell applications. *Renew. Sust. Energ. Rev.* **82**, 761-780 (2018).
3. D. Pakhare, J. Spivey, A review of dry (CO2) reforming of methane over noble metal catalysts. *Chem. Soc. Rev.* **43**, 7813-7837 (2014).
4. P. Serna, A. Corma, Transforming Nano Metal Nonselective Particulates into Chemoselective Catalysts for Hydrogenation of Substituted Nitrobenzenes. *ACS Catal.* **5**, 7114-7121 (2015).
5. K. Morgan, A. Goguet, C. Hardacre, Metal Redispersion Strategies for Recycling of Supported Metal Catalysts: A Perspective. *ACS Catal.* **5**, 3430-3445 (2015).
6. S. B. Simonsen *et al.*, Direct Observations of Oxygen-induced Platinum Nanoparticle Ripening Studied by In Situ TEM. *J. Am. Chem. Soc.* **132**, 7968-7975 (2010).
7. J. Im, M. Choi, Physicochemical Stabilization of Pt against Sintering for a Dehydrogenation Catalyst with High Activity, Selectivity, and Durability. *ACS Catal.* **6**, 2819-2826 (2016).
8. L. Liu *et al.*, Evolution and stabilization of subnanometric metal species in confined space by in situ TEM. *Nat. Comm.* **9**, Article number 574 (2018).
9. T. Otto, S. I. Zones, E. Iglesia, Challenges and strategies in the encapsulation and stabilization of monodisperse Au clusters within zeolites. *J. Catal.* **339**, 195-208 (2016).
10. M. Moliner *et al.*, Reversible Transformation of Pt Nanoparticles into Single Atoms inside High-Silica Chabazite Zeolite. *J. Am. Chem. Soc.* **138**, 15743-15750 (2016).
11. L. Liu *et al.*, Generation of subnanometric platinum with high stability during transformation of a 2D zeolite into 3D. *Nat. Mater.* **16**, 132-138 (2017).
12. S. Li *et al.*, Hollow Zeolite Single-Crystals Encapsulated Alloy Nanoparticles with Controlled Size and Composition. *ChemNanoMat* **2**, 534-539 (2016).
13. J. J. H. B. Sattler *et al.*, Platinum-Promoted Ga/Al2O3 as Highly Active, Selective, and Stable Catalyst for the Dehydrogenation of Propane. *Angew. Chem. Int. Ed.* **53**, 9251-9256 (2014).
14. A. Corma, H. García, Crossing the borders between homogeneous and heterogeneous catalysis: developing recoverable and reusable catalytic systems. *Topics Catal.* **48**, 8-31 (2008).
15. C. Ratnasamy, J. P. Wagner, Water Gas Shift Catalysis. *Catal. Rev.* **51**, 325-440 (2009).
16. J. Jones *et al.*, Thermally stable single-atom platinum-on-ceria catalysts via atom trapping. *Science* **353**, 150-154 (2016).
17. C. Paolucci *et al.*, Dynamic multinuclear sites formed by mobilized copper ions in NOx selective catalytic reduction. *Science* **357**, 898-903 (2017).
18. L. DeRita *et al.*, Catalyst Architecture for Stable Single Atom Dispersion Enables Site-Specific Spectroscopic and Reactivity Measurements of CO Adsorbed to Pt Atoms, Oxidized Pt Clusters, and Metallic Pt Clusters on TiO2. *J. Am. Chem. Soc.* **139**, 14150-14165 (2017).
19. K. Narsimhan, K. Iyoki, K. Dinh, Y. Roman-Leshkov, Catalytic Oxidation of Methane into Methanol over Copper-Exchanged Zeolites with Oxygen at Low Temperature. *ACS Cent. Sci.* **2**, 424-429 (2016).
20. M. Choi, Z. Wu, E. Iglesia, Mercaptosilane-Assisted Synthesis of Metal Clusters within Zeolites and Catalytic Consequences of Encapsulation. *J. Am. Chem. Soc.* **132**, 9129-9137 (2010).

21. M. Moliner, A. Corma, General Aspects on Structure and Reactivity of Framework and Extra-framework Metals in Zeolite Materials. *Struct. Bond.* **DOI: 10.1007/430_2017_21**, (2018).
22. P. Vanelderen, J. Vancauwenbergh, B. F. Sels, R. A. Schoonheydt, Coordination chemistry and reactivity of copper in zeolites. *Coord. Chem. Rev.* **257**, 483-494 (2013).
23. M. Chen, L. D. Schmidt, Morphology and sintering of Pt crystallites on amorphous SiO2. *J. Catal.* **55**, 348-360 (1978).
24. P. Lööf, B. Stenbom, H. Nordén, B. Kasemo, Rapid Sintering in NO of Nanometer-Sized Pt Particles on γ-Al2O3 Observed by CO Temperature-Programmed Desorption and Transmission Electron Microscopy. *J. Catal.* **144**, 60-76 (1993).
25. S. Porsgaard *et al.*, Stability of Platinum Nanoparticles Supported on SiO2/Si(111): A High-Pressure X-ray Photoelectron Spectroscopy Study. *ACS Nano.* **6**, 10743-10749 (2012).
26. A. I. Frenkel, Q. Wang, S. I. Sanchez, M. W. Small, R. G. Nuzzo, Short range order in bimetallic nanoalloys: An extended X-ray absorption fine structure study. *J. Chem. Phys.* **138**, 064202 (2013).
27. T. W. Hansen, A. T. DeLaRiva, S. R. Challa, A. K. Datye, Sintering of Catalytic Nanoparticles: Particle Migration or Ostwald Ripening? *Acc. Chem. Res.* **46**, 1720-1730 (2013).
28. B. Ravel, M. J. Newville, ATHENA, ARTEMIS, HEPHAESTUS: data analysis for X-ray absorption spectroscopy using IFEFFIT. *Synchrotron Radiat.* **12**, 537-541 (2005).
29. S. I. Zabinsky, J. J. Rehr, A. Ankudinov, R. C. Albers, M. Eller, Multiple-scattering calculations of x-ray-absorption spectra. *J. Phys. Rev. B: Condens. Matter Mater. Phys.* **52**, 2995−3009 (1995).